Heliyon 10 (2024) e23531

Contents lists available at ScienceDirect

Heliyon

journal homepage: www.cell.com/heliyon

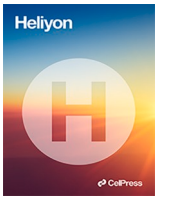

Isolation, purification, and antiosteoporosis activity of donkey bone collagen from discarded bone and its antioxidant peptides

Jie Wang [a,b,c,d], Huiwen Hou [a,c,d], Yan Li [a,c,d], Wen Tang [a,c,d], Didi Gao [a,c,d], Zengmei Liu [a,c,d], XinQing Gao [a,c,d], Feiyan Zhao [a,c,d], Feng Sun [a,c,d], Haining Tan [a,c,d,e], Juan Wang [f,*]

[a] National Glycoengineering Research Center, Shandong University, Qingdao, 266237, China
[b] Qingdao Haier Biotech Co., Ltd., Qingdao, 266237, China
[c] NMPA Key Laboratory for Quality Research and Evaluation of Carbohydrate-Based Medicine, Shandong University, Qingdao, 266237, China
[d] Shandong Provincial Technology Innovation Center of Carbohydrate, Shandong University, Qingdao, 266237, China
[e] School of Pharmaceutical Sciences, Shandong University, Jinan, 250012, China
[f] Jinan Maternity and Child Care Hospital Affiliated to Shandong First Medical University, Jinan, 250001, China

ARTICLE INFO

Keywords:
Donkey bone collagen
Osteoporosis
Oxidative stress
Antioxidant
Polypeptides

ABSTRACT

Oxidative stress plays a crucial role in the development of osteoporosis. In this study, it was observed that donkey bone collagen (DC) at a concentration of 500 μg/mL scavenged 17.89 % of 1,1-Diphenyl-2-picrylhydrazyl (DPPH) free radicals, indicating its antioxidant properties. Additionally, when an oxidative damage osteoblast model was created using H_2O_2, 100 μg/mL DC demonstrated the ability to enhance cell survival by 27.31 %. Furthermore, 50 μg/mL DC increased the intracellular differentiation marker alkaline phosphatase (ALP) level by 62.65 %. Additionally, the study revealed that DC significantly increased the expression of osteoporosis-related factors in serum and effectively restored the abnormal structure of spongy bone in mice osteoporosis model. Peptides (GGWFL, ANLGPA, and GWFK) isolated from DC through gastrointestinal digestion and subsequent enzymatic purification *in vitro* demonstrated the ability to safeguard osteoblasts from H_2O_2-induced damage by reducing intracellular reactive oxygen species (ROS). This protection resulted in enhanced cell survival and promoted osteoblast differentiation. This investigation underscores that DC can shield oxidative damage osteoblast model from oxidative stress, ameliorate osteoporosis, and enhance bone density in mice osteoporosis model. These findings suggest various DC applications in the food and medicine industries.

1. Introduction

The skeletal environment operates as a stable system under the regulations of osteoblasts, osteocytes, and osteoclasts, which continuously remodel it to mend micro-damage and respond to mechanical and metabolic demands [1]. The main underlying cause of osteoporosis is the disruption of this steady-state environment, leading to diminished bone formation, elevated bone resorption, and, ultimately, decreased bone density [2]. The prevalence and economic impact of osteoporosis are expected to increase in the coming

* Corresponding author. Jinan Maternity and Child Care Hospital Affiliated to Shandong First Medical University, Jinan, 250001, Shandong, China.
E-mail address: smartjww@126.com (J. Wang).

https://doi.org/10.1016/j.heliyon.2023.e23531
Received 12 May 2023; Received in revised form 5 December 2023; Accepted 5 December 2023
Available online 13 December 2023

years, with most patients being women [3]. Compared to conditions like myocardial infarction, stroke, and breast cancer, osteoporosis has a higher incidence rate among women, imposing a significant burden on families and society at large [3,4]. Osteoporosis is often described as a silent disease with no apparent clinical signs in its early stages [5]. However, as the condition progresses, changes in the patient's bone microstructure can lead to pain and gradually impede daily life [1]. Therefore, it is crucial to focus on the prevention, early detection, and timely treatment of osteoporosis [1,6].

Many studies have demonstrated a strong connection between oxidative stress and osteoporosis. An intermediary redox state may suggest a synchronised interaction among osteoblasts, osteoclasts, and osteocytes, maintaining a balanced bone metabolism [7]. The equilibrium in bone metabolism can be disrupted by aging, estrogen deficiency, radiation exposure, chronic inflammation, and various other influences [7–9]. Among elderly individuals diagnosed with primary osteoporosis, there is a notable elevation in oxidative stress levels [10]. Furthermore, in patients with postmenopausal osteoporosis, a significant and inverse correlation exists between the oxidative stress index and bone density of the lumbar spine and femoral neck [11]. An excessive burden of reactive oxygen species (ROS) can impair cell differentiation, resulting in osteoblastic dysfunction, diminished bone formation, and, ultimately, bone loss [8,9]. Reports indicate that superoxide anions generated by osteoclasts can break down bone matrix proteins even without enzymes, which renders bone matrix proteins vulnerable to degradation by associated enzymes [12]. Antioxidants enhance osteoporosis treatment by either neutralising the effects of oxidants or fostering osteoblastic differentiation while inhibiting osteoclast differentiation [13].

Collagen is a structural protein that forms the foundation of the extracellular matrix, boasting a triple helix structure, and it is abundant in various body parts, such as the skin, tendons, bones, ligaments, and numerous organs [14]. Collagen exhibits a range of biological functions, including antioxidant, antihypertensive, anti-inflammatory, immune regulation, wound healing, and more [14]. Because of these properties, it finds extensive applications in food, nutrition, health, cosmetics, materials, textiles, and beyond [15]. Recent reports have indicated that the supplementation of collagen and peptides can enhance bone quality, bone mineral density, bone microstructure, and bone metabolism in rats with surgical-induced ovarian removal [16]. This supplementation has demonstrated the ability to impede bone loss and act as a preventive measure against osteoporosis [16,17].

China possesses abundant animal bone resources, and these bones are notably rich in collagen, comprising approximately 80 %–90 % of their composition [18]. The effectiveness of collagen peptides is influenced by several factors, including their amino acid composition, hydrophobicity, molecular weight, structure, and other physical and chemical properties [19]. The collagen peptides' capacity to chelate and neutralise free radicals is intimately connected to the presence of certain amino acids such as Ala, Gly, Pro, Cys, Tyr, and Met [20,21]. It has been found that collagen peptides from cod skin can have the potential to attenuate oxidative stress, thus reversing osteoblast dysfunction and mitigating osteoporosis [22]. Additionally, bone collagen and its hydrolysed peptides have effectively improved osteoporosis [17,18].

In recent years, the utilisation rate of bone collagen from animals like pigs, cattle, sheep, and others has experienced a decline. This decrease in attributed factors such as disease outbreaks like avian influenza, foot-and-mouth disease, mad cow disease, and religious considerations [18]. Conversely, the utilisation of bone collagen sourced from aquatic animals like fish, squid, and jellyfish has increased [18]. Nevertheless, the relatively low levels of proline and hydroxyproline in collagen from aquatic animals result in reduced thermal stability, limiting the potential application of marine animal collagen [23].

Donkey bones are a valuable source of collagen; however, they are often discarded as by-products when processing other donkey products like donkey skins and donkey meat. This leads to significant environmental pollution and represents a waste of valuable resources [24]. Previous research has demonstrated that collagen extracted from donkey bones can efficiently neutralise DPPH free radicals and hydroxyl radicals, showcasing specific antioxidant properties, and it has shown promise in improving osteoporosis [24,25]. This study aimed to explore the potential anti-osteoporosis properties of donkey bone collagen (DC) isolated from discarded donkey bone and its antioxidant constituents on *in vitro* and *in vivo* osteoporosis models. This study offers fresh insights into the development and utilisation of donkey bone resources and serves as a stepping stone for future investigation into antioxidant and anti-osteoporosis medications.

2. Materials and methods

2.1. Materials

Donkey leg bones (Dezhou donkey) were procured from Dong-E-E-Jiao Co., Ltd., Liaocheng, China. MC3T3-E1-subclone 14 cells, derived from mice cranial parietal pre-osteocyte, were acquired from Chunmai Biotechnology, Shanghai, China. KM mice were purchased from Chengdu Dashuo Laboratory Animal Co., Ltd. (SCXK (Chuan) 2020-030). Common maintenance feed was sourced from Keao Xieli (Tianjin) Feed Co., Ltd. Low calcium feed was purchased from Xiaoshu Youtai (Beijing) Biotechnology Co., Ltd. (SCXK (Beijing) 2018-0006).

The following materials and reagents were acquired from Beijing Solarbio Science & Technology Co., Ltd., Beijing, China: EDTA-Na_2, flavourzyme (endopeptidases, exopeptidases), high-sugar DMEM medium, phosphate-buffered saline (PBS), ascorbic acid, sodium β-glycerophosphate, dexamethasone, DEAE-52 cellulose, L-Glutathione (Reduced, GSH), and 2′-Azinobis-(3-ethylbenzthiazoline-6-sulphonate) (ABTS). Fetal bovine serum (FBS) was obtained from Zhejiang Tianhang Biotechnology Co., Ltd., Huzhou, China. Penicillin-streptomycin, N-Acetyl-L cysteine (NAC), and CCK-8 solution were received from Genview Scientific Inc., Florida, USA. The BCA kit, DCFH-DA solution, BCIP/NBT dyeing solution, ALP kit, and malondialdehyde (MDA) kit were obtained from Beyotime Biotechnology Co., Ltd., Nanjing, China. Paraformaldehyde (4 %) was obtained from Servicebio Technology Co., Ltd., Wuhan, China. D-galactose and potassium persulfate were received from Macklin Biochemical Technology Co., Ltd., Shanghai, China. Osteoprotegerin

(OPG) kit, osteocalcin (OCN) kit, tartrate-resistant acid phosphatase (TRAP) kit, and superoxide dismutase (SOD) kit were obtained from Mlbio Biotechnology Co. Ltd., Shanghai, China. Sephadex G25 was sourced from GE Healthcare, Sweden. The protein marker was procured from SMOBIO. DPPH was obtained from Aladdin Biochemical Technology Co., Ltd., Shanghai, China. ANLGPA (AA-6) peptide, HYFL (HL-4) peptide, PAEGPA (PA-5) peptide, KLLHA (KA-5) peptide, HVPNA (HA-5) peptide, GGWFL (GL-5) peptide, and GWFK (GK-4) peptide were received from Baige Pharmaceutical Technology Co., Ltd., Hangzhou, China. All other reagents were purchased from Sinopharm Chemical Reagents in Shanghai, China.

2.2. Methods

2.2.1. Extraction and characterization of donkey collagen

A sequence of solutions, including 0.1 M NaOH, n-hexane, and 0.25 M EDTA-Na_2 (pH 7.4), was added to the cleaned donkey bone block in a 5:1 (v/w) ratio to remove non-collagen elements, lipids, and calcium salts from the donkey bone. Afterward, distilled water was added to 10 times the donkey bone's weight. The mixture was stirred in an oil bath at 140 °C for 3 h. After cooling, flavourzyme was added at a mass ratio of 0.1 % (enzyme to mixture), and the collagen solution was obtained by subjecting it to enzymatic digestion at 60 °C for 1 h, followed by enzyme inactivation at 140 °C for 1 h. The donkey bone collagen (DC) was subsequently separated by centrifugation of the supernatant and then freeze-dried. Finally, the concentration of protein in DC was determined using a BCA kit, and the structure properties of DC were analysed through UV, IR, and SDS-PAGE.

2.2.2. In vitro cell experiments

2.2.2.1. Cell viability assay (CCK-8). In the experiment, a complete medium was prepared, consisting of a high-sugar DMEM medium supplemented with 10 % fetal bovine serum and 1 % penicillin-streptomycin. MC3T3-E1 cells in their logarithmic growth phase were then seeded into a 96-well plate at a density of 1×10^4 cells/well. After cell attachment, fresh media containing various DC concentrations (150, 100, 50, 20, 10, and 5 μg/mL, 100 μL/well) were added to 96-well plates and incubated at 37 °C for 24 h. Then, the medium was removed, and the 96-well plate underwent two washes with fresh medium. Subsequently, fresh medium (100 μL/well) was added, followed by a CCK-8 reaction solution (10 μL/well). Subsequently, the plate was incubated for 1–2 h in a light-free environment. After incubation, the absorbance at 450 nm was measured using a microplate reader.

2.2.2.2. Establishment of oxidative damage cell model. MC3T3-E1 cells in the logarithmic growth phase were seeded into a 96-well plate at a density of 1×10^4 cells/well. They were then placed in a cell incubator for 6–8 h to allow for adherence. After this initial adherence period, the cells were incubated for 24 h. The old medium was discarded, and fresh medium with different H_2O_2 concentrations (800, 700, 600, 500, 400, 300, 200, 100, 50 μmol/L) was added to the plate (100 μL/well) and incubated for 4 h. After incubation, the plate was washed twice with fresh medium. Finally, the fresh medium was added to the 96-well plate (100 μL/well). Cell survival rate was then measured using a CCK-8 solution.

2.2.2.3. Protective effect of DC on oxidative damage cell model. MC3T3-E1 cells in the logarithmic growth were seeded into a 96-well plate at a density of 1×10^4 cells/well. After the cells had adhered to the well, fresh media containing different concentrations of DC (150, 100, 50, 20, 10, and 5 μg/mL, 100 μL/well) were introduced. The plate was then incubated at 37 °C for 24 h, and a fresh medium containing H_2O_2 (300 μmol/L, 100 μL/well) was added. The mixture was incubated for 4 h. Afterward, the medium was discarded, and the 96-well plate underwent two washes with fresh medium. Finally, fresh medium (100 μL/well) was added, and the cell survival rate was determined using a CCK-8 solution.

2.2.2.4. Detection of intracellular ROS. This experiment employed a 12-well cell plate with a seeding density of 1×10^5 cells/well. The DC concentrations were 100, 50, and 20 μg/mL. The initial steps of intracellular ROS detection followed the same protocol as in the earlier experiment, which investigated the protective effects of DC on the oxidative damage cell model. After discarding the old medium containing H_2O_2 following a 4 h incubation, the MC3T3-E1 cells underwent two washes with fresh medium. Then, a DCFH-DA solution (at 10 μmol/L in serum-free medium, 1 mL/well) was added. The 12-well plate was incubated in a darkened cell incubator for 20–30 min. In the subsequent step, the cells were collected, washed 2 to 3 times with PBS to eliminate any excess DCFH-DA solution, and resuspended in PBS. The levels of ROS in each group were assessed using a flow cytometer (FITC channel).

2.2.2.5. Qualitative detection of intracellular ALP. To prepare the osteoblast differentiation medium, ascorbic acid (50 μg/mL), sodium β-glycerophosphate (10 mmol/), and dexamethasone (100 nmol/L) were added to the complete medium. Cells of the logarithmic growth stage were seeded into a 12-well plate at a density of 1×10^4 cells/well. Once the cells had adhered to the well, the old medium was removed, and the fresh complete medium was added to the blank control well, the osteoblast differentiation medium was added to the differentiation culture control well and the oxidative damage model control well, and the differentiation medium containing DC (50 μg/L) was added to the DC treatment group, and the differentiation medium containing NAC (163 μg/mL) was added to the positive control well (1 mL/well). The medium was changed every 2–3 days and maintained 7 days. Subsequently, the medium was removed, and 300 μmol/L H_2O_2 was added to the 12-well plate (1 mL/well). The mixture was then incubated in a cell incubator for 4 h. After the incubation, the old medium was discarded, and the 12-well plate underwent two washes with PBS. After washing, 4 % paraformaldehyde was added to each well of the 12-well plate (500 μL/well). The cells were fixed at 4 °C for 15 min. The

paraformaldehyde was discarded, and the plate was rinsed twice with deionised water to remove the residual paraformaldehyde. An appropriate amount of BCIP/NBT dyeing solution was added to each well of the 12-well plate (enough to cover the bottom) to complete the process. The plate was then incubated at room temperature away from light until the desired color developed was achieved. Once the color had developed to the expected level, the dyeing solution was removed, and the 12-well plate was washed 1 to 2 times with distilled water. The staining results were photographed and recorded by microscope and camera.

2.2.2.6. Quantitative detection of intracellular ALP. The initial steps of the experiment reflected those used in the qualitative detection of intracellular ALP indicated earlier. After washing the 12-well plate with PBS, the cells were lysed in the lysate solution (the lysate should not contain phosphatase inhibitors), and then the cells were harvested using a cell scraper. The next step involved the collection of the supernatant through centrifugation, followed by quantifying ALP content in each group using the ALP quantitative detection kit.

2.2.3. In vivo experiments

The animal experiments adhered to the guidelines established by the National Institute for the Care and Use of Laboratory Animals. All experimental procedures received approval from the Laboratory Animal Ethical and Welfare Committee at Shandong University Cheeloo College of Medicine. The ethical approval number of these animal experiments is SYXK(Lu): 20190005.

An animal model of osteoporosis with oxidative stress was established by administering D-galactose (D-Gal) with a low-calcium diet [27]. To assess the success of osteoporosis modeling, bone mass and bone histopathology were used as evaluation criteria [26,27]. After 5 days of adaptive feeding, fifty female KM mice (weighing 34.48 ± 1.37 g) were randomly divided into five groups: the blank group (Con), the model group (D-Gal), the DC low-dose group (DC 0.6), the DC medium-dose group (DC 1.2), and the DC high-dose group (DC 2.4), each consisting of 10 mice. In the blank group, mice had a standard maintenance diet containing 1 %–1.8 % calcium. They received subcutaneous injections of normal saline (1 mL/kg b.w.) and were administered distilled water by gavage (2 mL/kg b.w.) daily for 20 days. For the other groups, mice were subcutaneously injected with a 12.5 % D-galactose solution (1 mL/kg b.w.) in the back of the mouse near the neck and were fed a low-calcium diet containing 0.1 % calcium daily for 20 days. The DC low, middle, and high dose groups received doses of 0.6 g/kg, 1.2 g/kg, and 2.4 g/kg, respectively, based on their body weight, and this was administered by gavage (2 mL/kg b.w.) daily for 20 days.

Following the final intragastric administration, the mice underwent a 12-h fasting period, during which their last recorded weights were measured. Initially, blood samples were collected from the mouse's socket. After that, the mice were sacrificed by stripping their necks. Subsequently, the heart, liver, spleen, lung, and kidney were dissected, and their respective weights were recorded. Following this, the right femur was carefully extracted and preserved in tissue fixative, with special attention paid to preserving the integrity of the distal femoral trabecular bone.

Mice blood samples were utilised to assess various bone turnover indicators, including osteoprotegerin (OPG), osteocalcin (OCN), tartrate-resistant acid phosphatase (TRAP), and oxidative stress indexes malondialdehyde (MDA), and superoxide dismutase (SOD). Additionally, the right femur underwent micro-computed tomography (Micro CT, Bruker, Germany) analysis to evaluate the bone mineral density and microstructure of the mice. Micro CT analysis utilised the following conditions: 18 μm resolution, 50 kV voltage, 455 μA current, 265 ms exposure time. CTvox software was employed for the 3D reconstruction of bone tissue. CTAn software was used to quantitatively analyse bone parameters, including bone mineral density, bone volume fraction, trabecular thickness, trabecular space, trabecular number, and trabecular pattern factors.

2.2.4. In vitro simulated gastrointestinal digestion of DC

2.2.4.1. In vitro simulated gastrointestinal digestion. 1 g of DC was dissolved in 75 mL distilled water. Following this, 28.57 mg of pepsin was added at a ratio of 1:35 (enzyme to protein, w/w). The pH was then carefully adjusted to 2.00 ± 0.02, and the mixture was subjected to shaking for 1 h at 37 °C and 150 rpm/min. Subsequently, the pH was adjusted to 7.00 ± 0.02 to end the pepsin reaction. Then, 75 mL of distilled water was introduced, and 40 mg of trypsin was added at a ratio of 1:25 (enzyme to protein, w/w). The mixture was shaken for 2 h at 37 °C and 150 rpm/min. To terminate the reaction, the reaction solution was subjected to a 15-min heating in a boiling water bath and then centrifuged at 8000 rpm/min for 15 min. The resulting supernatant, the enzymatic hydrolysate of DC (DCH), was collected for freeze-drying, and the protein content of DCH was assessed using the BCA kit.

2.2.4.2. Isolation and purification of DCH. DCH underwent a series of separation and purification steps, including ultrafiltration, anion exchange chromatography using DEAE-52 (dimensions: 3.5 cm × 13 cm), gel filtration chromatography using G-25 (dimensions: 3 cm × 100 cm), and reversed-phase high-performance liquid chromatography (HPLC, C-18, dimensions: 4.6 mm × 250 mm). These processes aimed to isolate and purify specific components. The screening of the component with the most potent antioxidant activity was based on its ability to scavenge DPPH free radicals.

Three components (DCH-a, DCH-b, and DCH-c) of varying molecular weights were initially obtained via ultrafiltration (MW: 3 kDa and 10 kDa). DCH-c, possessing higher scavenging activity, was selected for subsequent purification. DCH-c was then purified using a DEAE-52 cellulose anion exchange column and eluted stepwise with distilled water, as well as NaCl solutions at concentrations of 2 mM, 5 mM, 10 mM, 50 mM, and 100 mM. The purification process involved a flow rate of 5 mL/min, with detection at 214 nm. Five components were separated and collected: DCHc-A, DCHc-B, DCHc-C, DCHc-D, and DCHc-E. Among these, DCHc-A exhibited higher scavenging activity and underwent further purification using G-25 gel size exclusion chromatography. This purification was carried out with distilled water as the eluent at a flow rate of 2 mL/min, with detection at 214 nm. Four components were obtained and named

DCHcA-1, DCHcA-2, DCHcA-3, and DCHcA-4. Subsequently, DCHcA-3 was purified using an HPLC column. Distilled water was used as phase A, and acetonitrile was employed as phase B. A gradient elution was conducted, transitioning from 5 %–30 % phase B, with a flow rate of 0.4 mL/min for 20 min. Fractions showing absorbance at 214 nm were collected freeze-dried, isolating two components, DCHcA3-α and DCHcA3-β. DCHcA3-α, displaying superior scavenging activity, was selected for mass spectrometry sequencing. Peptides derived from DCHcA3-α were synthesised via solid-phase synthesis, and their purity was assessed using HPLC.

2.2.4.3. Prediction of isoelectric points. The isoelectric points of the peptides were forecasted and assessed using the online protein analysis tool ProtParam, available at http://web.expasy.org/protparam.

2.2.4.4. Scavenging activity of DPPH radicals. A mixture was prepared by combining 125 μL of ethanol containing DPPH radicals (0.02 %) with 500 μL of the products obtained during purification. The mixture was then incubated in the dark at room temperature for 1 h, after which the absorbance (A_s) of the samples was measured at 517 nm. A control group, A_c, was used as the blank without any sample, while GSH was the positive control. The inhibition rate of each sample towards DPPH free radical was calculated using Eq. (1).

$$\text{Clearance rate } (\%) = (1 - A_s/A_c) \times 100\% \quad (1)$$

2.2.4.5. Scavenging activity of hydroxyl radicals. Polypeptides, synthesised using 100 μL through solid-phase synthesis, were mixed with 30 μL of an 8 mmol/L $FeSO_4$ solution, 100 μL of 3 mmol/L salicylic acid solution, and 25 μL of 20 mmol/L H_2O_2 solution. The total

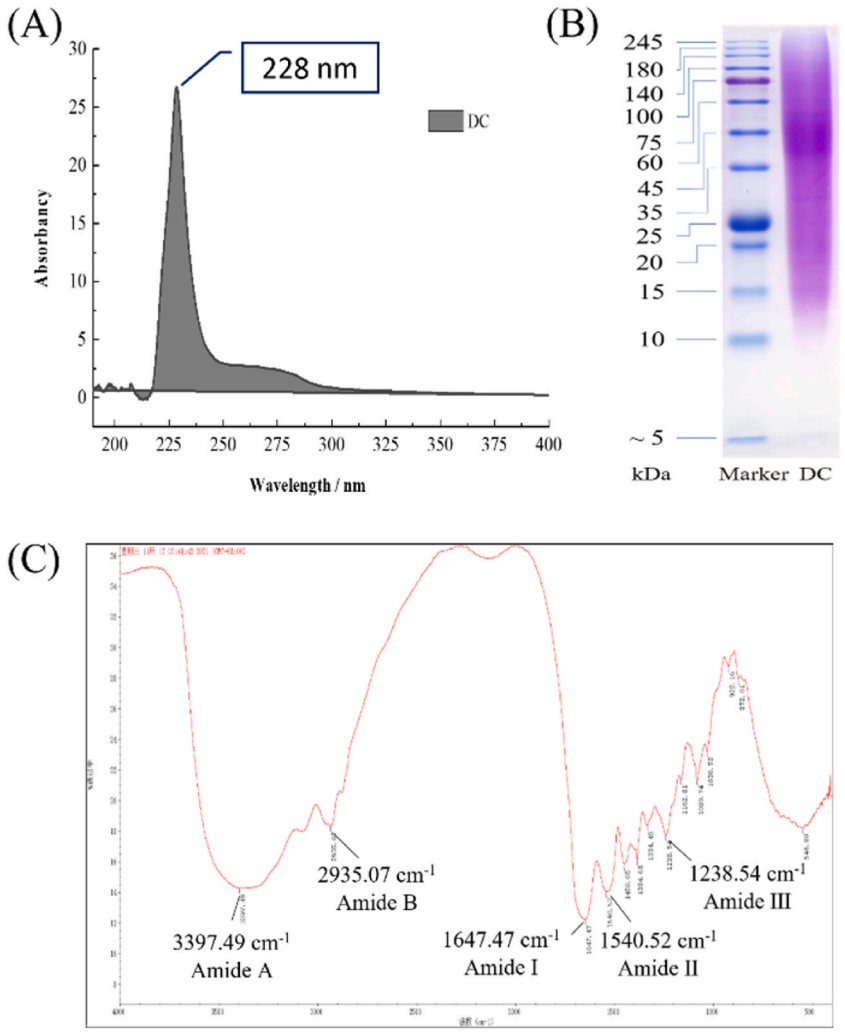

Fig. 1. Charact1erisation of donkey bone collagen (DC). (A) The UV absorption spectrum of DC. (B) SDS-PAGE profile of DC. (C) Infrared absorption spectrum of DC.

volume was then brought to 300 μL by adding distilled water. The reaction occurred at 37 °C for 30 min, after which it was allowed to cool to room temperature and subjected to centrifugation at 3000 rpm/min for 10 min. The absorbance of the sample was assessed at 510 nm (A_1) using the supernatant. For a negative control (A_2), only the sample was used without adding H_2O_2, while a blank control (A_0) was obtained in the absence of the sample. GSH served as the positive control. The scavenging rate of hydroxyl radicals for each

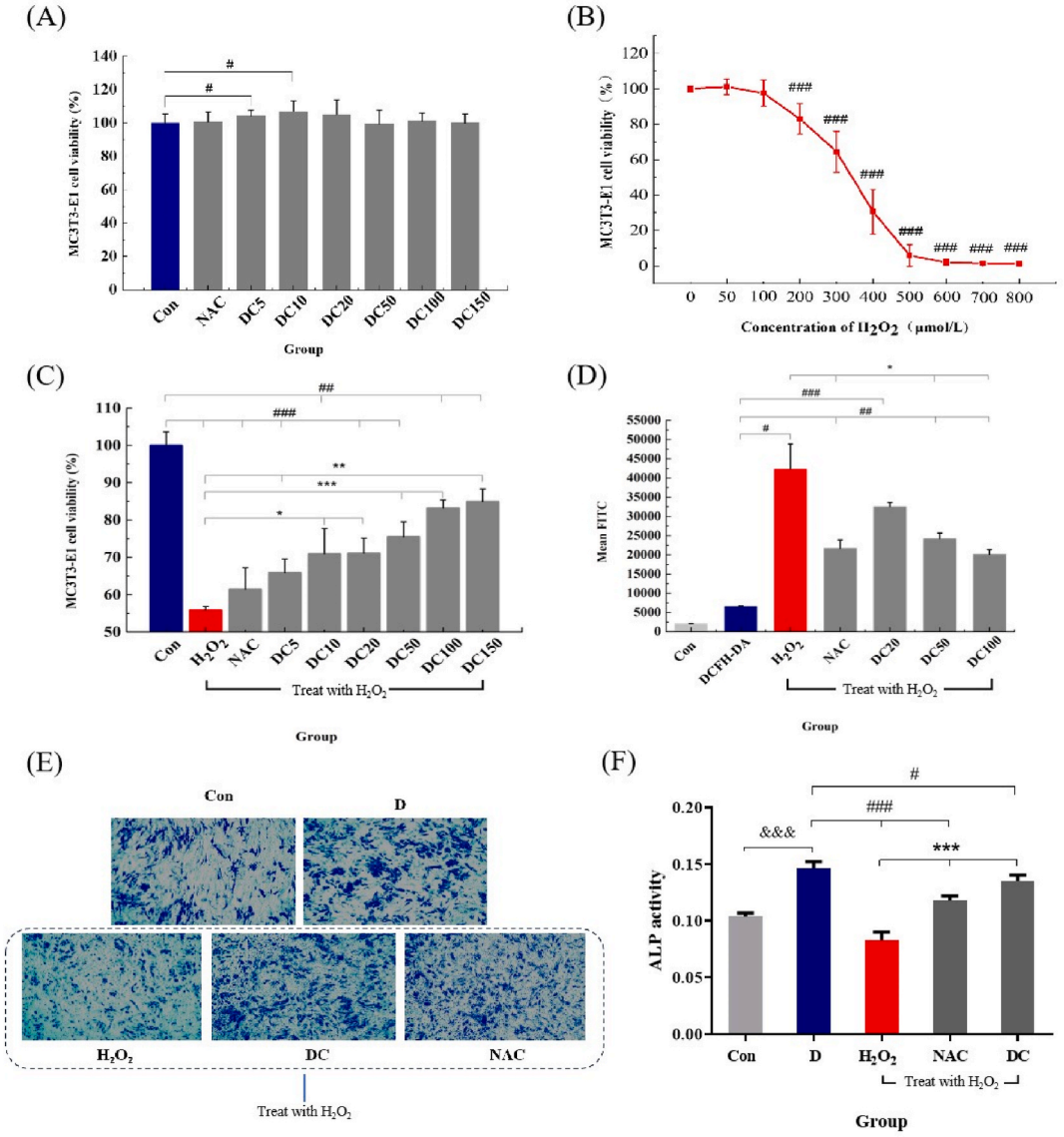

Fig. 2. Effects of donkey bone collagen (DC) on oxidative damage osteoblasts model. (A) The effect of DC on osteoblasts under various conditions. Con: a control group without any treatment, incubation 24 h without a sample; NAC: incubation with 163 μg/mL NAC for 24 h; DC5, DC10, DC20, DC50, DC100, and DC150: incubation with different concentrations of DC, respectively 5, 10, 20, 50, 100, and 150 μg/mL for 24 h. **(B)** The effect of H_2O_2 on osteoblasts under various conditions. **(C)** The protective effect of DC on MC3T3-E1. H_2O_2 model: incubation with 300 μmol/L H_2O_2 alone; NAC: incubation with 163 μg/mL NAC followed by incubation with H_2O_2; DC5, DC10, DC20, DC50, DC100, and DC150: incubations with DC at concentrations of 5, 10, 20, 50, 100, and 150 μg/mL, respectively, followed by incubation with H_2O_2. **(D)** DC and its impact on intracellular ROS levels. DCFH-DA: blank control group involving incubation with DCFH-DA alone. H_2O_2: model group featuring incubation with H_2O_2, followed by DCFH-DA incubation. NAC: incubation with 163 μg/mL NAC, followed by H_2O_2, and then DCFH-DA incubation. DC20, DC50, and DC100: Incubation with DC at concentrations of 20, 50, and 100 μg/mL, respectively, followed by H_2O_2 and then DCFH-DA incubation. **(E)** Influence of DC on intracellular ALP levels. **(F)** Semi-quantitative analysis of intracellular ALP levels. Con: normal medium culture with incubation and no sample; D, differentiation medium culture with incubation and no sample; H_2O_2: model group in differentiation medium culture with incubation, exposed to H_2O_2 alone; NAC: differentiation medium culture with incubation in the presence of 163 μg/mL NAC, followed by exposure to H_2O_2; DC: differentiation medium culture with incubation in the presence of 50 μg/mL DC, followed by exposure to H_2O_2. Group D compared to Con, $^{\&\&\&}P < 0.001$; the experimental group compared with the blank group $^{\#}P < 0.05$, $^{\#\#}P < 0.01$, $^{\#\#\#}P < 0.001$; the experimental group compared with the model group $^{*}P < 0.05$, $^{**}P < 0.01$, $^{***}P < 0.001$.

sample was calculated using Eq. (2).

$$\text{Clearance rate } (\%) = [1 - (A_1\text{-}A_2)/A_0] \times 100\% \quad (2)$$

2.2.4.6. Scavenging activity of ABTS cations. Initially, a mixture was prepared by combining 5 mL of 7 mmol/L stock solution 2′-Azinobis-(3-ethylbenzthiazoline-6-sulphonate) (ABTS) with 5 mL of a 2.45 mmol/L potassium persulfate solution. This mixture was left in a dark room at room temperature for 16 h to generate an ABTS cationic solution. The ABTS cationic solution was diluted with 5 mmol/L PBS until the absorbance at 734 nm fell within the range of 0.70 ± 0.02. Following this, 100 μL of the solid-phase synthesised polypeptides were combined with 100 μL of the ABTS cationic solution and incubated at room temperature for 10 min. Each sample group's absorbance (A_s) was determined at 734 nm using a microplate reader. A control group without any sample, A_c, was used as a blank reference, and GSH was employed as the positive control. The scavenging rate of each sample against ABTS cations was determined using Eq. (1).

2.2.4.7. Scavenging activity of superoxide anions. A mixture was prepared by combining the following components with the sample (all the solid-phase synthesis polypeptides, 50 μL): Nitrotetrazolium Blue chloride (50 μL, 72 μM), β-Nicotinamide adenine dinucleotide (50 μL, 338 μM), and phenazine methosulfate (50 μL 30 μM). The mixture was incubated for 5 min at room temperature. Subsequently, the absorbance (A_s) of the samples at 560 nm was measured. A blank group, devoid of any sample, was employed as the blank control (A_c), and GSH served as the positive control. The scavenging rate of ABTS cations for each sample was calculated using Eq. (1).

2.2.5. Statistical analysis

All experimental results were presented as Mean ± SD (standard deviation). Data processing and analysis were conducted using statistical software such as Excel, SPSS 22.0, and Image J. Group comparisons were carried out using one-way ANOVA. Fisher's least significant difference (LSD) method was employed for multiple comparisons between groups. Graphical analysis and visualisation were performed using GraphPad and Origin 2020 software tools.

3. Results and discussion

3.1. Characterization of DC

DC was extracted from donkey bone using an enzymatic method at high temperatures. The protein content in DC was determined to be 56 %, and DC exhibited its highest UV absorption at 228 nm (Fig. 1A), a characteristic absorption peak associated with collagen [28]. Notably, no distinct protein bands were observed within the range of 5 kDa and 245 kDa (Fig. 1B), and DC appeared a diffuse distribution. During the extraction of DC at elevated temperatures, the hydrogen bonds within the molecule undergo disruption, leading to the practical destruction of the triple helix structure. Consequently, this results in varying relative molecular masses of the polypeptide chains, causing DC to exhibit a dispersed relative molecular mass distribution. The infrared absorption spectrum of DC (Fig. 1C) indicates prominent bands, denoted as amide bands A (3397.49 cm^{-1}), B (2935.07 cm^{-1}), I (1647.47 cm^{-1}), II (1540.52 cm^{-1}), and III (1238.54 cm^{-1}). Typically, the free N–H group exhibits stretching vibrations within the range of 3400–3440 cm^{-1}. However, when the N–H groups within the peptide engage in hydrogen bonding, the wavenumber shifts to a lower frequency. In this case of DC, the absorption of amide band A is observed at 3397.49 cm^{-1}, indicating that certain N–H groups within DC are involved in forming hydrogen bonds. The appearance of amide band I in the range of 1600–1700 cm^{-1} primarily corresponds to C–O stretching vibration and is associated with the secondary structure of collagen. The absorption wavenumber of DC in this range signifies the presence of gelatin with a distinct coil conformation. The amide II bands, found within the wavenumber range of 1500–1600 cm^{-1}, arise from C–N stretching vibrations and N–H bending. Lower wavenumbers in the amide II bands indicate a greater prevalence of N–H hydrogen bonds and a higher degree of structural order. The absorption of the amide III band is associated with the content of collagen's Gly, Pro, and Hyp within collagen. DC's distinctive absorption peak sets it apart from other proteins, primarily due to C–N stretching and N–H bending vibrations linked to the CH_2 group in the Gly main chain and Pro side chain. This unique spectral feature reflects DC's partial retention of triple-helical structures and a specific degree of structural order.

3.2. Effect of DC on oxidative damage osteoblasts model

In this study, we generated an oxidative damage model for osteoblasts to investigate whether DC can protect osteoblasts from oxidative stress. Initially, it was confirmed that DC at concentrations ranging from 5 to 150 μg/mL did not exhibit any harmful effects on MC3T3-E1 cells, as shown in Fig. 2A. This allowed us to proceed with subsequent activity assays. Furthermore, H_2O_2 was selected as an inducer of cellular oxidative stress damage due to its chemical reactivity and efficient cell penetration and exit capabilities, making it an ideal choice [29]. Furthermore, it was observed that H_2O_2 concentrations ranging from 200 to 800 μmol/L substantially reduced cell viability ($P < 0.001$), as shown in Fig. 2B. Specifically, following a 4 h exposure to 300 μmol/L, the cell viability decreased to 64.44 %, thus establishing a model of oxidative stress injury in osteoblasts using 300 μmol/L H_2O_2. In the oxidative damage osteoblast model, pretreatment with DC at concentrations ranging from 5 to 150 μg/mL for 24 h enhanced cell viability, as illustrated in Fig. 2C. Notably, pretreatment with 150 μg/mL DC elevated cell viability to 84.94 %, a significant improvement compared to H_2O_2 treatment alone ($P <$

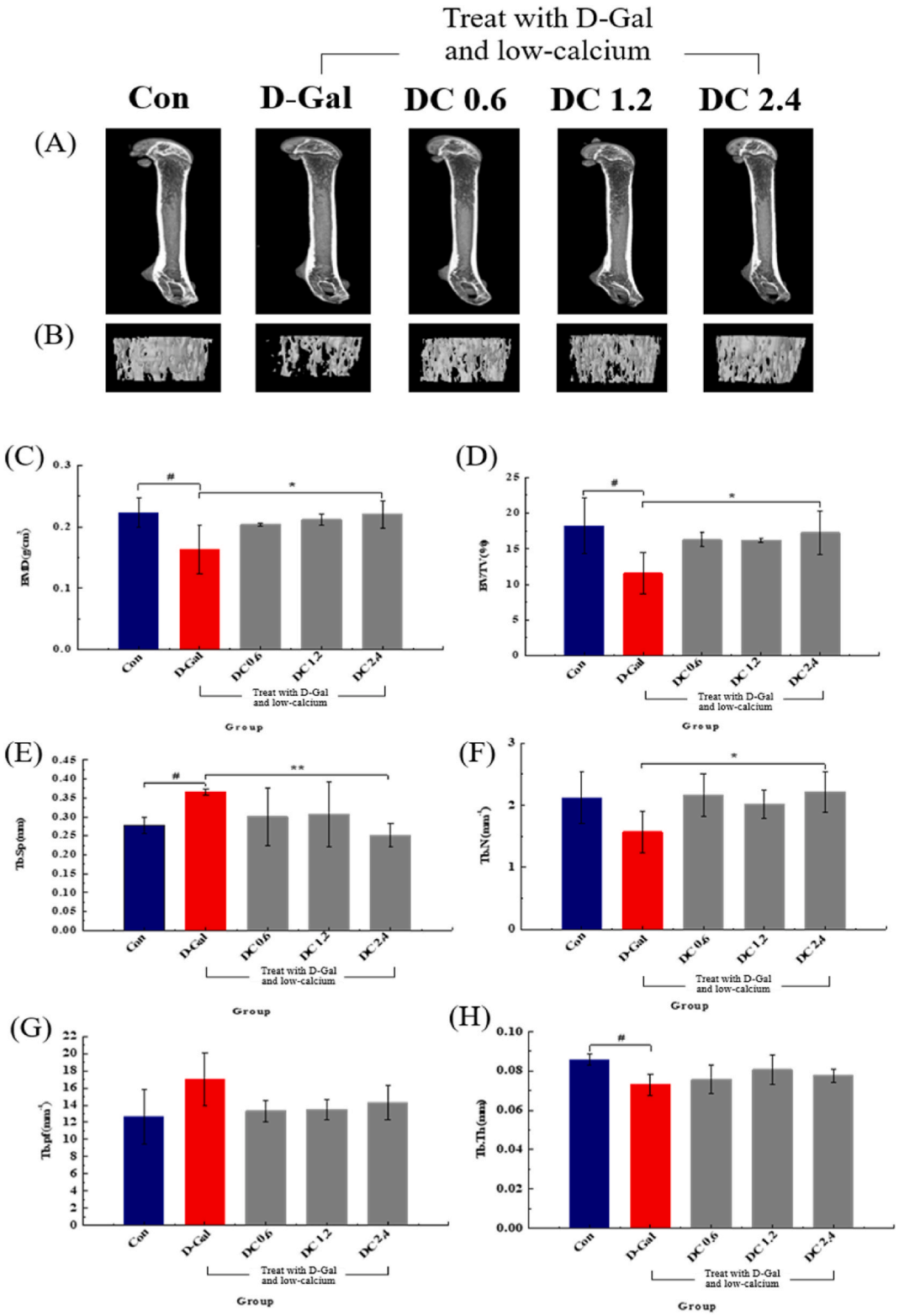

(caption on next page)

Fig. 3. Effect of donkey bone collagen (DC) on bone mineral density and bone microarchitecture in mice osteoporosis model. **(A)** Whole-mount 3D reconstruction of a mice femur sample. **(B)** 3D reconstruction of the cancellous region of the distal femur. **(C)** Changes in Mice Femur Bone Mineral Density (BMD, mg/m^3); **(D)**. Alterations in bone volume fraction (BV/TV, %). **(E)** Changes in trabecular bone separation (Tb. Sp, mm). **(F)** Variations in trabecular bone number (Tb. N, mm^{-1}). **(G)** Alterations in trabecular bone pattern factor (Tb. pf, mm^{-1}). **(H)** Changes in trabecular thickness (Tb. Th, mm). Legend signifies the treatment groups: the Con group, the control group received distilled water, underwent subcutaneous injections of normal saline, and was fed with a standard maintenance diet; D-Gal model, the subjects received oral gavage of distilled water, underwent subcutaneous injection with D-galactose, and were maintained on a low-calcium diet; the administration group was divided into three subgroups based on the dosage of DC: DC 0.6 g/kg, DC 1.2 g/kg, and DC 2.4 g/kg. These subgroups received DC through oral gavage at doses of 0.6, 1.2, and 2.4 g/kg, respectively, together with subcutaneous injections of D-galactose, and were maintained on a low-calcium diet. Dosing group compared with Con group: $^{\#}P < 0.05$, $^{\#\#}P < 0.01$, $^{\#\#\#}P < 0.001$; Dosing group compared with D-Gal group: $^{*}P < 0.05$, $^{**}P < 0.01$, $^{***}P < 0.001$.

0.01). Subsequent examination of intracellular ROS levels in each group (Fig. 2D) revealed that H_2O_2 treatment led to a notable increase in intracellular ROS levels in MC3T3-E1 cells. Conversely, pretreatment with 20, 50, and 100 μg/mL DC significantly lowered the intracellular ROS levels ($P < 0.05$).

To further assess the influence of DC on osteoporosis, cells were cultured in a differentiation medium, and the impact of DC on osteoblast differentiation was evaluated based on the differentiation marker ALP [30]. Qualitative analysis of ALP level in each group was performed using the BCIP/NBT chromogenic kit, as shown in Fig. 2E. The staining results were quantified using Image J, as depicted in Fig. 2F. The H_2O_2-treated group exhibited lighter ALP staining compared to the differentiation medium alone. In contrast, the DC-treated group displayed intensified ALP staining and increased ALP levels. These findings suggest that DC possesses distinct antioxidant properties, which enable it to shield MC3T3-E1 cells from H_2O_2-induced damage, enhance cell survival, and mitigate the abnormally elevated levels of intracellular ROS. Additionally, DC can elevate the bone formation marker ALP levels, stimulate osteoblast differentiation, and demonstrate potential as an anti-osteoporosis agent.

3.3. In vivo experiments

3.3.1. Effect of DC on bone mineral density and bone microstructure in mice osteoporosis model

The osteoporosis model was established by combining D-galactose and low-calcium feeding [27]. Bone densitometry, bone histomorphometry, blood and urine biochemical analysis, bone mechanics tests, body weight, gonadal morphology, etc., can be used to evaluate the success of the osteoporosis model. The primary indicators include bone mass and histopathological alterations [26]. Micro CT was conducted on the right femurs of the mice to provide a more intuitive observation of their skeletal condition. Micro CT enables 3D imaging analysis of samples without destructive measures and allows for clear differentiation of the trabecular bone structure [31]. When comparing the reconstructed femur image of the mice in the Con group to those in the D-Gal group, a significant reduction in cancellous bone was evident in the mice from the D-Gal group. The cancellous bone in this group also exhibited cavity, indicating the successful construction of an osteoporosis mouse model. Additionally, following DC intervention, the cancellous bone content in mice increased to varying degrees compared to the D-Gal group, suggesting an improvement in osteoporosis to some extent (Fig. 3A/B).

The diagnosis of osteoporosis primarily relies on the measurement of bone mineral density (BMD) to assess the mineral content of bones. Quantitative analysis of various morphometric parameters of mouse femur is conducted using relevant software. These parameters include BMD, bone volume fraction (BV/TV), trabecular bone number (Tb. N), trabecular bone thickness (Tb. Th), trabecular bone separation (Tb. Sp), and trabecular bone pattern factor (Tb. pf). Among these parameters, BMD serves as an indirect indicator of bone quality and strength. BV/TV, on the other hand, quantifies the ratio of bone tissue volume to the total volume and reflects bone mass. Increased BV/TV suggests that bone anabolism exceeds catabolism, increasing bone mass. Tb. N, Tb. Th and Tb. Sp are used to assess the spatial morphology of trabecular bone, Tb. Th represents the average thickness of trabecular bone, while Tb. Sp measures the width of the trabecular bone space and the average width of the medullary cavity between trabecular bone structures. Tb. pf indicates the concavity of the trabecular bone surface. This parameter characterises the proportion of lamellar and rod-like structures within the composition of trabecular bone. In cases of osteoporosis, there is a shift from plate-like to rod-like trabecular bone, increasing this value [32]. In the D-Gal mice group, BMD (Fig. 3C), BV/TV (Fig. 3D), Tb. N (Fig. 3F) and Tb. Th (Fig. 3H) decreases by 27.27 %, 36.53 %, 25.94 %, and 15.12 %, respectively. Conversely, Tb. Sp (Fig. 3E) and Tb.pf (Fig. 3G) increased by 32.14 % and 33.91 %, respectively. The reduced bone density led to a decrease in bone mass, and the density of trabecular bone declined. Additionally, the bone structure shifted from rod-like to plate-like, damaging the bone microstructure. Following the administration of varying concentrations of DC, an improvement in the mice's bone microstructure was observed. Notably, after the intervention of 2.4 g/kg DC, there were significant enhancements in BMD, BV/TV, and Tb. N, and Tb. Th increased by 27.27 %, 49.18 %, 41.40 %, and 6.85 %, respectively. In contrast, Tb. Sp and Tb.pf decreased by 32.43 % and 15.67 %. These changes indicated an increase in bone density and mass, a reduction in trabecular space, and a shift in bone structure from plate-like to rod-like. The overall improvement in the bone microstructure contributed to the repair of abnormal cancellous bone structure.

3.3.2. Effect of DC on the body and organ weight in mice osteoporosis mice

An excessive injection of D-galactose leads to an increase in the body's galactitol content. Galactitol cannot undergo further cellular metabolism and accumulates rapidly in tissue cells. Consequently, cells cannot maintain normal osmotic pressure, resulting in cell swelling, metabolic disruptions, and functional impairment. An ongoing and intensified oxidative stress response is associated with the increased production of substantial amounts of ROS [33]. Notably, the mice continued to gain weight throughout the administration period, as shown in Fig. 4A. After the experiment, the rate of weight gain in the model group (D-Gal) was significantly higher than that

in the blank group (Con) ($P < 0.05$). However, compared to the model group, the rate of weight gain in the mice decreased in the groups treated by DC.

The quality and organ index of internal organs serves as key biological characteristics of experimental animals. These parameters are valuable for assessing the animals' functional status in biomedical research, providing insights into their growth, development stages, physiological conditions, and environmental adaptability [34]. Compared to the mice in the Con group, the liver index of D-Gal mice showed a significant increase ($P < 0.05$), as depicted in Fig. 4C. The liver is a crucial organ involved in the metabolism of various substances, and it serves as the site for generating free radicals and lipid peroxidation. Subcutaneous injection of D-galactose leads to elevated levels of peroxides within the body [35]. Free radicals covalently bind to macromolecules within liver cells, including unsaturated fatty acids in cell membranes. This process triggers lipid peroxidation, raises the permeability of liver cell membranes, induces cell swelling necrosis, and ultimately results in increased fat content within liver tissue [36]. Following treatment with various

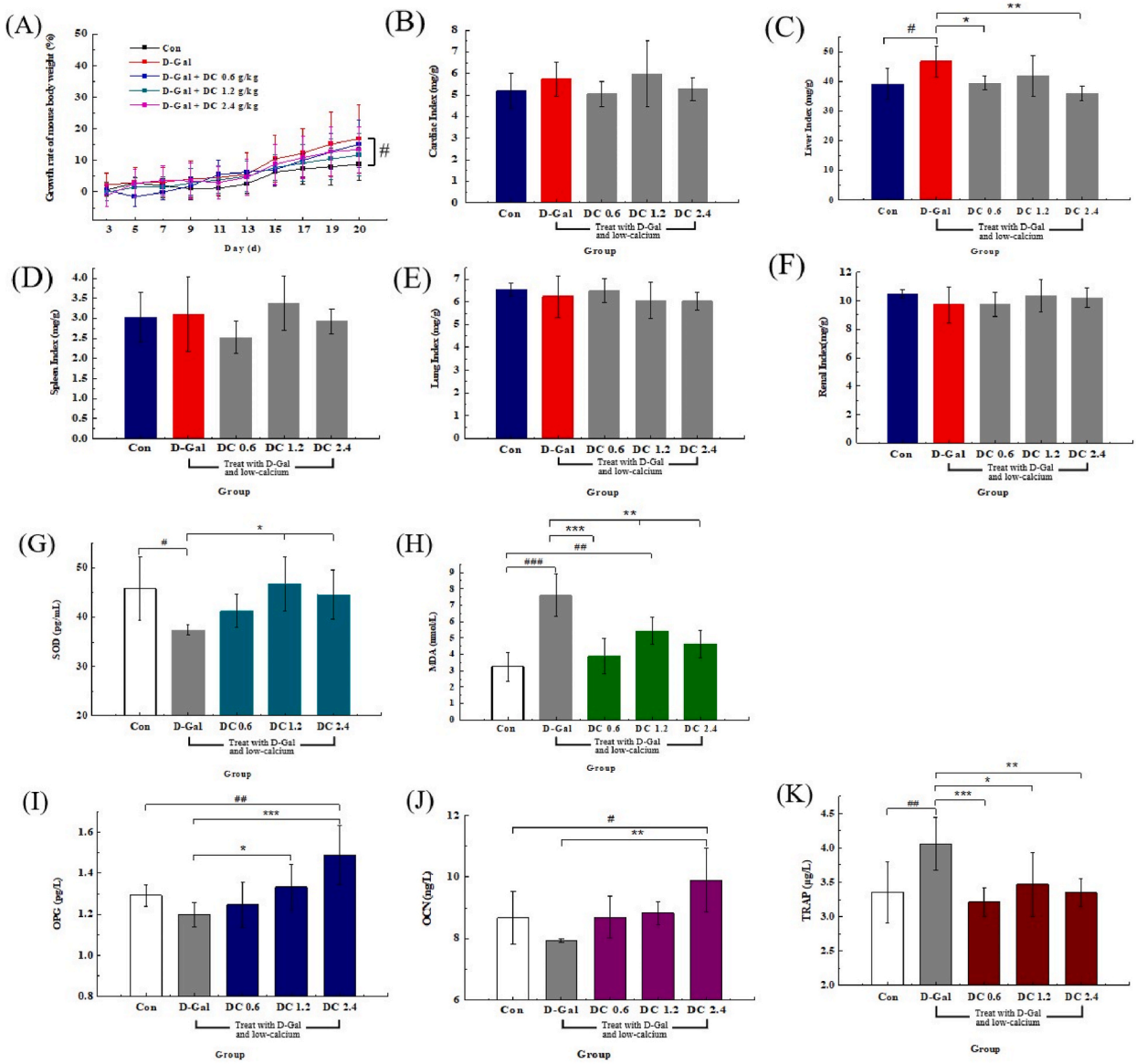

Fig. 4. Effect of donkey bone collagen (DC) on body weight, organ index, and biochemical indexes in mice osteoporosis model. (A) Body weight growth rate of mice. **(B)** Cardiac index. **(C)** Liver index. **(D)** Spleen index. **(E)** Lung index. **(F)** Renal index. **(G)** SOD level in mice serum. **(H)** MDA level in mice serum. **(I)** OPG levels in mice serum. **(J)** OCN levels in mice serum. **(K)** TRAP levels in mice serum. The Con group, which served as the blank control, received distilled water administration, subcutaneous injections of normal saline, and was provided with a standard maintenance diet; D-Gal model group: was subjected to oral gavage with distilled water, subcutaneous injection of D-galactose, and were placed on a low-calcium diet; administration group where three subgroups received different doses of DC: 0.6 g/kg, 1.2 g/kg, and 2.4 g/kg, together with subcutaneous injections of D-galactose and were maintained on a low-calcium diet. The D-Gal group compared with the Con group, $^{\#}P < 0.05$.

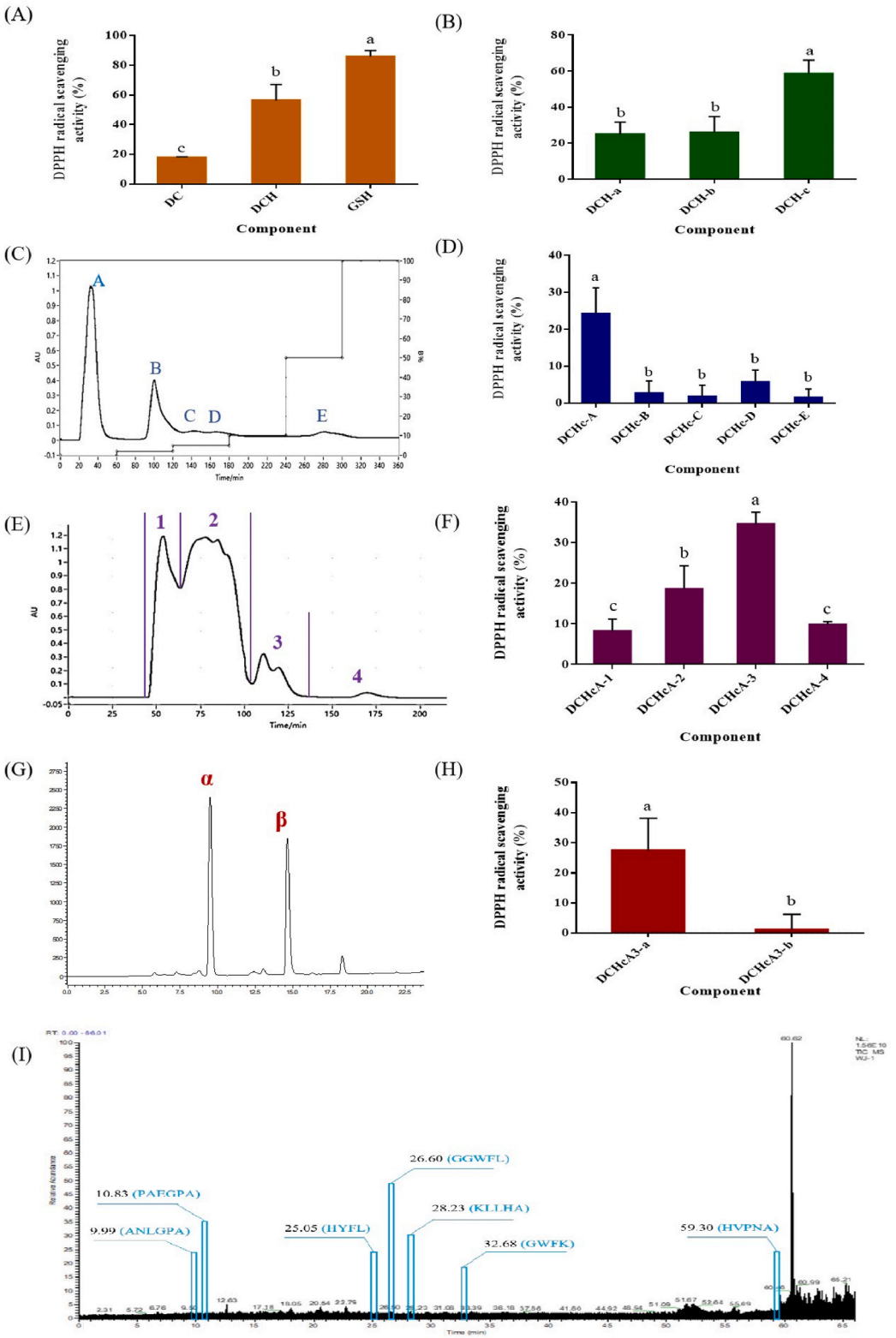

Fig. 5. The antioxidant activity of the enzymatic hydrolysate of donkey bone collagen (DCH) and its purification process. (A) Scavenging activities of DC, DCH, and GSH on DPPH free radicals. **(B)** DPPH radical scavenging rate of DCH-a with MW > 10 kDa, DCH-b with 10 kDa > MW > 3 kDa, DCH-c with MW < 3 kDa. **(C)** The elution curve of DCH-c through anion exchange chromatography. **(D)** Scavenging activity of each component obtained through anion exchange elution on DPPH free radical. **(E)** The elution pattern of DCHc-A through G-25 gel size exclusion

chromatography. **(F)** Scavenging activity of each component eluted by G-25 gel size exclusion chromatography against DPPH free radical. **(G)** The elution pattern of DCHcA-3 through C18 reversed-phase HPLC column. **(H)** Scavenging activity of each component eluted by the C18 reversed-phase HPLC column against DPPH free radical. **(I)** LC-MS/MS detection of the total ion chromatogram.

concentrations of DC, the liver index in mice decreased. DC effectively reduced fat accumulation in mice livers and mitigated D-galactose-induced damage. Notably, apart from the liver index, the indexes of other organs, such as the cardiac, spleen, lung, and renal, did not show significant changes. D-galactose and DC treatment did not significantly damage these organs (Fig. 4B/D/E/F).

3.3.3. Effect of DC on oxidative stress and bone transition levels in mice osteoporosis model

D-galactose combined with a low-calcium diet led to a reduction in SOD level ($P < 0.05$) in the D-Gal group (Fig. 4G) and a significant increase in MDA level ($P < 0.001$) (Fig. 4H). Treatment with different concentrations of DC significantly increased SOD activity, and reduced MDA levels thus DC exerted antioxidant effects and countered oxidative stress damage to the body.

OCN, a non-collagen protein, is abundantly present in bone tissue and primarily synthesised by osteoblasts, chondrocytes, and odontoblasts. Osteoblast-secreted OCN plays a crucial role in the regulation of bone mineralisation, as well as in glucose and lipid metabolism and calcium homeostasis. During bone resorption, collagenase-hydrolysed products generated by TRAP within these vesicles are eventually released outside the cell. Hence, serum TRAP is a more accurate indicator of osteoclast bone resorption activity [37]. In comparison to the Con group, the levels of OCN (Fig. 4J) and OPG (Fig. 4I) were reduced in the D-Gal group, while the level of TRAP (Fig. 4K) significantly increased ($P < 0.05$). These findings indicate a decrease in the bone formation capacity of mice and a substantial increase in the bone resorption ability. In comparison to D-Gal-treated mice, the levels of OCN and OPG were significantly increased ($P < 0.05$), while the level of TRAP was significantly decreased ($P < 0.05$) in DC-treated mice (DC 0.6, DC 1.2, and DC 2.4). These results indicate that bone resorption decreased considerably after DC intervention treatment. DC exhibited clear effects in inhibiting bone resorption and promoting bone formation.

3.4. In vitro simulation of DC gastrointestinal digestion and isolation and purification of enzymatic lysates

Initial experiments have indicated that administering DC via gavage can ameliorate osteoporosis in mice. However, it is known that oral DC can be digested in the gastrointestinal tract. To understand the active compounds generated by DC in the body, we simulated *in vitro* gastrointestinal digestion of DC. Our goal was to investigate whether DC can combat osteoporosis through its antioxidant properties and identify active components in the enzymatic hydrolysate of DC using antioxidant activity as a screening criterion. The enzymatic hydrolysate of DCH (56.35 %) exhibited significantly higher antioxidant activity compared to DC (17.89 %) (Fig. 5A). Gastrointestinal digestion unleashed the inherent antioxidant potential of DC. The preliminary infrared spectroscopy results indicated that DC still retained a certain triple helix structure. DC contains stable structural components organised in a triple helix structure when dissolved in an aqueous solution. Within this structure, active groups between the peptide chains form stable hydrogen bonds, either directly or indirectly, concealed within the triple helix. Consequently, the antioxidant activity of DC is relatively lower than DCH [38].

The DCH-c fraction, obtained through ultrafiltration, demonstrated the highest scavenging activity against DPPH radicals (Fig. 5B), reaching 58.59 %. This activity was significantly superior to that of DCH-a and DCH-b. It has been reported in previous studies that peptides with shorter chain lengths more readily capture free radicals. Therefore, fractions with smaller molecular weights exhibit stronger antioxidant activity than those with larger molecular weights [39,40]. The DCH-c fraction, obtained through ultrafiltration, was subjected to elution using an anion exchange column with mobile phases consisting of distilled water, 2 mM, 5 mM, 10 mM, 50 mM, and 100 mM NaCl solutions, respectively (Fig. 5C). The scavenging activity of each component against DPPH free radicals at a concentration of 500 μg/mL was assessed (Fig. 5D). Among these components, DCHc-A, eluted with distilled water, exhibited the highest scavenging activity against DPPH free radicals (24.18 %, $P < 0.05$).

DCHc-A, which was enriched, underwent further purification using a G-25 gel column (Fig. 5E). The scavenging activity of DPPH free radicals of each component at a concentration of 500 μg/mL was assessed. The results revealed that DCHcA-3 exhibited significantly higher scavenging activity against DPPH free radicals compared to the other three components (34.59 %, $P < 0.05$) (Fig. 5F).

DCHcA-3 underwent further enrichment and was subjected to C18 purification, resulting in two fractions, DCHcA3-α and DCHcA3-β (Fig. 5G). The DPPH free radical scavenging activity of these two components was assessed, and DCHcA3-α exhibited higher scavenging activity than DCHcA3-β (Fig. 5H), with a rate of 27.49 %. DCHcA3-α was then enriched for LC-MS/MS sequencing. Using

Table 1
LC-MS/MS sequencing.

Peptide	Score	*m/z*	*z*	Area	Mass	ppm
A (+42.01) NLGPA	77	584.3045	1	1.96E+05	583.2966	1.1
HYFL	74	579.2935	1	2.43E+07	578.2853	1.7
P (+42.01) AEGPA	71	583.2660	1	3.27E+04	582.2649	−10.6
KLLHA	68	291.1958	2	1.14E+05	580.3697	12.6
H (+42.01) VPNA	62	579.2941	1	6.01E+06	578.2812	9.6
GGWFL	61	579.2932	1	3.75E+06	578.2853	1.0
G (+42.01) WFK	60	579.2943	1	5.00E+06	578.2853	2.9

Xcalibur to analyse the total electron flow pattern generated by LC-MS/MS detection (Fig. 5I), seven peptides were identified (Table 1), with the following sequences: ANLGPA (AA-6), HYFL (HL-4), PAEGPA (PA-6), KLLHA (KA-5), HVPNA (HA-5), GGWFL (GL-5), and GWFK (GK-4).

3.5. Characterization and antioxidant activity of antioxidant peptides obtained by in vivo digestion of DC

The solid phase analysis has produced seven peptides. HPLC analysis shows that AA-6, HL-4, PA-6, KA-5, HA-5, GL-5, and GK-4 have purities 95.43 %, 96.52 %, 99.30 %, 96.47 %, 98.78 %, 96.47 %, and 97.27 %, respectively, where all above 95 %. Nanodrop UV absorption measurements indicate that these peptides primarily exhibited absorption peaks at 220 nm, representing peptide bond absorption peaks. HL-4, GL-5, and GK-4, which contain aromatic amino acids, display higher absorption peaks at 280 nm. The isoelectric points of the seven peptides were determined using ProtParam. The isoelectric points of each peptide are 5.57 (AA-6), 6.74 (HL-4), 4.00 (PA-6), 8.76 (KA-5), 6.74 (HA-5), 5.52 (GL-5), and 8.75 (GK-4). Subsequently, the antioxidant activities of these seven peptides were assessed based on their scavenging abilities against DPPH radicals, hydroxyl radicals, ABTS cations, and superoxide anions.

At the concentration of 1 mg/mL, the scavenging activities of the peptides HA-5, GK-4, KA-5, AA-6, GL-5, PA-6, and HL-4 on DPPH free radicals were found to be 22.90 % and 34.05 %, 27.10 %, 49.46 %, 43.23 %, 22.06 %, and 6.15 % respectively (Fig. 6A). Notably, AA-6 and GL-5 exhibit relatively strong scavenging activities against DPPH free radicals at higher concentrations. AA-6 (ANLGPA) contains hydrophobic amino acid Ala at both the amino and carboxyl termini, along with hydrophobic amino acids Leu, Pro, and Gly within the sequence. On the other hand, GL-5 (GGWFL) consists entirely of hydrophobic and aromatic amino acids, contributing to its high scavenging activity against DPPH free radicals.

Due to carboxyl and amino groups on their side chains, polar amino acids have been recognised for their important roles in scavenging hydroxyl radicals and chelating metal ions, and thus peptides composed of Glu, Arg, and Asp are particularly effective in chelating metal ions and neutralising hydroxyl radicals [41]. Among the peptides studied, AA-6 exhibited superior scavenging activity against hydroxyl radicals at a concentration of 250 μg/mL. Additionally, KA-5 and HA-5 demonstrated enhanced hydroxyl radical scavenging activities at concentrations exceeding 250 μg/mL (Fig. 6B). At a concentration of 1 mg/mL, KA-5 displayed slightly lower scavenging activity than the GSH group, registering at 24.05 %. At the same time, HA-5 exhibited a scavenging activity of 19.79 %. KA-5 (KLLHA) and HA-5 (HVPNA) contain many polar amino acids, contributing to their specific scavenging activity against hydroxyl radicals at higher concentrations.

At the concentration of 10 μg/mL, HL-4, GL-5, and GK-4 demonstrated scavenging rates of 35.91 %, 52.50 %, and 37.57 % against ABTS cations. These peptides exhibited effective ABTS cation scavenging even at lower concentrations (Fig. 6C). AA-6 exhibited a noteworthy scavenging ability against ABTS cations, and its efficacy displayed a concentration-dependent gradient. However, PA-6,

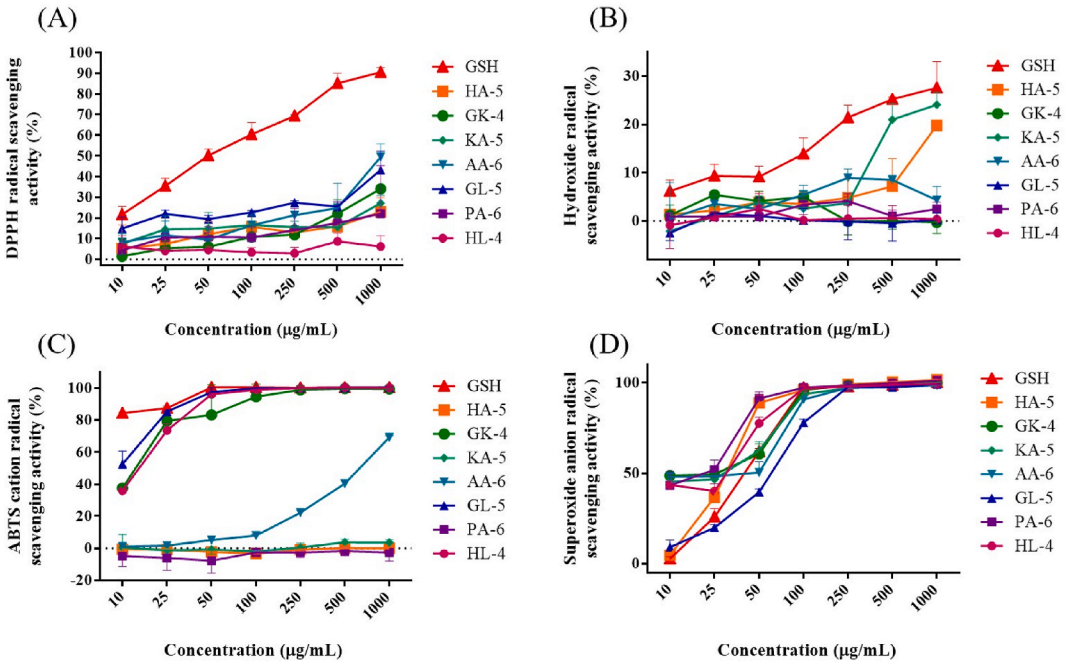

Fig. 6. Antioxidant activity of seven short peptides isolated from donkey bone collagen (DC). (A) The scavenging activity of seven short peptides was assessed by DPPH free radicals. **(B)** The scavenging activity of seven short peptides was assessed by hydroxyl radicals. **(C)** The scavenging activity of seven short peptides was assessed by ABTS cations. **(D)** The scavenging activity of seven short peptides was assessed by superoxide anion.

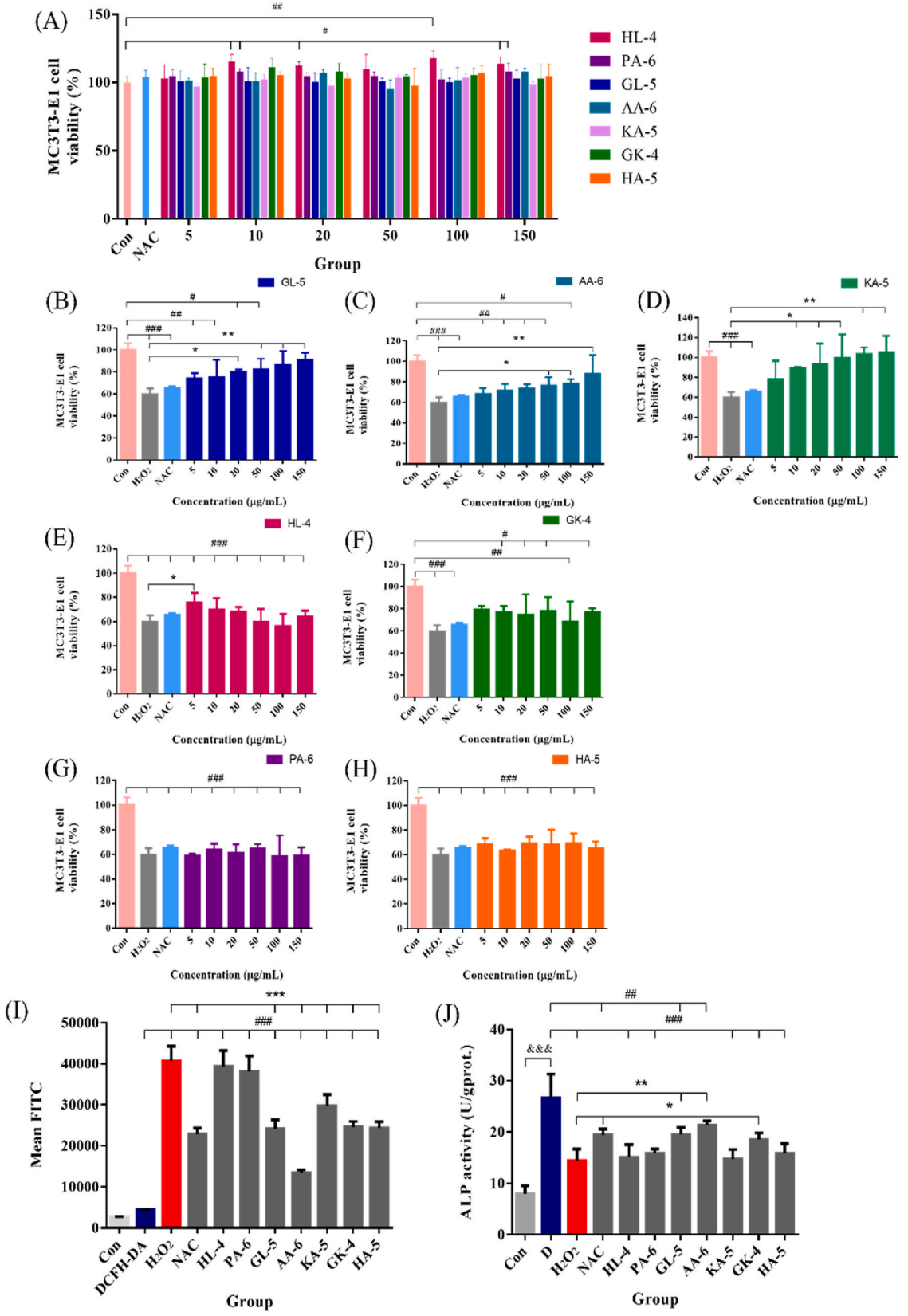

(caption on next page)

Fig. 7. Effects of seven short peptides on oxidative damage osteoblast model. **(A)** The effect of seven kinds of short peptides on MC3T3-E1. **(B)** The protective effect of GL-5 on MC3T3-E1. **(C)** The protective effect of AA-6 on MC3T3-E1. **(D)** The protective effect of KA-5 on MC3T3-E1. **(E)** The protective effect of HL-4 on MC3T3-E1. **(F)** The protective effect of GK-4 on MC3T3-E1. **(G)** The protective effect of PA-6 on MC3T3-E1. **(H)** The protective effect of HA-5 on MC3T3-E1. Con, blank control group, no drug incubation; H_2O_2, incubation with 300 μmol/L H_2O_2 alone; NAC, incubation with 163 μg/mL NAC, then H_2O_2 incubation. **(I)** Intracellular ROS levels in each group. DCFH-DA, blank control group, incubated with DCFH-DA alone; H_2O_2, model, incubated with H_2O_2, then DCFH-DA incubation; NAC, incubation with 163 μg/mL NAC, H_2O_2 incubation, then DCFH-DA incubation; HL-4, PA-6, GL-5, AA-6, KA-5, GK-4, HA-5, 50 μg/mL HL-4, PA-6, GL-5, AA-6, KA-5, GK-4, HA-5 pre-incubation, H_2O_2 incubation, then DCFH-DA incubation. **(J)** Intracellular ALP levels in each group. Con, normal medium culture, incubation with no sample; D, differentiation medium culture, incubation with no sample; H_2O_2, model, differentiation medium culture, incubation with H_2O_2 alone; NAC, differentiation medium culture, incubation with 163 μg/mL NAC, then incubation with H_2O_2; HL-4, PA-6, GL-5, AA-6, KA-5, GK-4, HA-5, differentiation medium culture, 50 μg/mL HL-4, PA-6, GL-5, AA-6, KA-5, GK-4, HA-5 incubation, then incubation with H_2O_2. Group D compared to Con, $^{\&\&\&}P < 0.001$; The experimental group compared with the blank group, $^{\#}P < 0.05$, $^{\#\#}P < 0.01$, $^{\#\#\#}P < 0.001$; The experimental group compared with the model group, $^{*}P < 0.05$, $^{**}P < 0.01$, $^{***}P < 0.001$.

KA-5, and HA-5 exhibited no discernible scavenging effect on ABTS cations. The peptides HL-4 (HYFL), GL-5 (GGWFL), and GK-4 (GWFK) contain a higher proportion of aromatic amino acids, while PA-6 (PAEGPA), KA-5 (KLLHA), and HA-5 (HVPNA) lack aromatic amino acids. Although AA-6 (ANLGPA) lacks aromatic amino acids, it possesses a substantial content of hydrophobic amino acids. Consequently, the scavenging ability of these peptides against ABTS cations may be attributed to the presence of hydrophobic and aromatic amino acids.

At lower concentrations, all seven short peptides demonstrated effective scavenging of superoxide anion, with scavenging ability exhibiting a concentration-dependent gradient (Fig. 6D). Specifically, at a concentration of 250 μg/mL, these peptides achieved a 100 % scavenging rate against superoxide anion. Consequently, all seven short peptides exhibited robust scavenging activity against superoxide anion, particularly at lower concentrations.

3.6. Effect of antioxidant peptides derived from the digestion of DC on oxidative damage osteoblasts model

The seven short peptides showed no toxicity to osteoblasts at various concentrations (Fig. 7A). HL-4 and PA-6 had moderate stimulating effects on cell proliferation. When treated with HL-4 and PA-6 at a concentration of 150 μg/mL, cell viability remained at 113.79 %, and 108.23 %, respectively. GL-5, AA-6, and KA-5 demonstrated concentration-dependent protection of osteoblasts from hydrogen peroxide-induced damage (Fig. 7B/C/D). HL-4 and GK-4 could also offer protection against hydrogen peroxide injury to osteoblasts (Fig. 7E/F). HL-4 significantly increased cell viability at a lower concentration of 5 μg/mL ($P < 0.05$) but had no protective effect on MC3T3-E1 at high concentrations. PA-6 and HA-5 did not protect oxidative damage osteoblast model, resulting in significantly lower cell viability than the blank group ($P < 0.05$) (Fig. 7G/H). GL-5, AA-6, KA-5, GK-4, and HL-4 peptides exhibited varying degrees of protection against hydrogen peroxide-induced osteoblast damage, indicating their potential anti-osteoporosis effects.

The impact of seven peptides on oxidative damage osteoblast model was investigated by quantitatively analysing intracellular peroxide levels in each group. H_2O_2 exposure significantly raised intracellular ROS content, but pretreatment with seven peptides could variably lower ROS levels (Fig. 7I). Compared with the model group, GL-5, AA-6, KA-5, GK-4, and HA-5 treatment groups decreased the intracellular ROS content by 40.67 %, 67.12 %, 26.81 %, 39.70 %, and 40.31 %, respectively, with significant difference ($P < 0.05$). GL-5, AA-6, KA-5, GK-4, and HA-5 could safeguard osteoblasts from oxidative damage by decreasing intracellular ROS levels. Among them, AA-6 demonstrated the most potent intracellular ROS scavenging effect, potentially offering osteoporosis resistance. HA-5 can reduce intracellular ROS levels but did not notably improve cell viability. This suggests that HA-5 can directly eliminate intracellular ROS but may not actively activate the cell's endogenous antioxidant pathways and promote the transcription of various cell protection genes [42].

In comparison to the Con group, the intracellular ALP levels in the differentiation culture group (D) were significantly elevated ($P < 0.001$), demonstrating that the differentiation medium effectively promoted osteoblast differentiation (Fig. 7J). H_2O_2 exposure inhibited osteoblast differentiation and reduced ALP activity, leading to increased ALP activity. GL-5, AA-6, and GK-4 treatments significantly elevated intracellular ALP levels ($P < 0.05$) compared to the H_2O_2 incubation group, promoting osteoblast differentiation. Combined, GL-5, AA-6, and GK-4 significantly increased the osteoblast survival rates, reduced cellular ROS levels, and promoted osteoblast differentiation compared to the H_2O_2-treated group. These peptides protect cells from H_2O_2-induced damage by diminishing cellular ROS levels, enhancing cell viability, and promoting osteoblast differentiation.

4. Conclusion

This study was initiated by extracting collagen (DC) from donkey bone to investigate its potential in mitigating oxidative stress-mediated osteoporosis. We made noteworthy findings through a series of *in vivo* and *in vitro* experiments. DC exhibited remarkable antioxidant properties, effectively ameliorating oxidative stress-induced damage to osteoblasts. Furthermore, when administered to mice with oxidative stress-induced osteoporosis, DC displayed a capacity to reduce oxidative stress levels, restore bone mineral density, and combat osteoporosis. Of particular significance are the seven antioxidant peptides we identified within DC. DDWFL, ANLGPA, and GWFK emerged as potent antioxidants, offering protective effects against hydrogen peroxide-induced osteoblast damage and promoting osteoblast differentiation. These findings underscore the promising potential of both DC and its enzymatic components in improving osteoporosis and advancing our understanding of its treatment options.

Data availability statement

Data will be made available on request.

CRediT authorship contribution statement

Jie Wang: Writing - original draft, Software, Project administration, Methodology, Investigation, Data curation. **Huiwen Hou:** Writing - review & editing, Supervision, Software, Data curation, Conceptualization. **Yan Li:** Writing - review & editing, Supervision, Software, Data curation. **Wen Tang:** Methodology, Data curation. **Didi Gao:** Methodology, Data curation. **Zengmei Liu:** Methodology, Data curation. **XinQing Gao:** Methodology, Data curation. **Feiyan Zhao:** Methodology, Data curation. **Feng Sun:** Writing - review & editing, Supervision, Formal analysis, Conceptualization. **Haining Tan:** Writing - review & editing, Supervision, Resources, Project administration, Investigation, Funding acquisition, Formal analysis, Conceptualization. **Juan Wang:** Writing - review & editing, Supervision, Resources, Project administration, Investigation, Funding acquisition, Formal analysis, Conceptualization.

Declaration of competing interest

The authors declare the following financial interests/personal relationships which may be considered as potential competing interests:Haining Tan, Feng Sun, Jie Wang, Huiwen Hou, Yan Li, Wen Tang, Zengmei Liu, Didi Gao has patent #202210885147.8 issued to Shandong University. If there are other authors, they declare that they have no known competing financial interests or personal relationships that could have appeared to influence the work reported in this paper.

Acknowledgments

This study was supported by the National Key Research and Development Program of China (2023YFF1103600), Key Research and Development Program of Shandong Province, China (2021CXGC010501), Fundamental Research Funds for the Central Universities, China (2022JC026), Youth Foundation of Shandong Natural Science Foundation, China (ZR2022QH134), Tai Mountain Industry Leading Talent of Shan Dong and Qilu Young Scholar Fund of Shandong University, China.

References

[1] R. Eastell, T.W. O'Neill, L.C. Hofbauer, B. Langdahl, I.R. Reid, D.T. Gold, et al., Postmenopausal osteoporosis, Nat. Rev. Dis. Prim. 2 (2016), 16069, https://doi.org/10.1038/nrdp.2016.69.
[2] L.G. Raisz, Pathogenesis of osteoporosis: concepts, conflicts, and prospects, J. Clin. Invest. 115 (12) (2005) 3318–3325, https://doi.org/10.1172/JCI27071.
[3] L. Si, T.M. Winzenberg, Q. Jiang, M. Chen, A.J. Palmer, Projection of osteoporosis-related fractures and costs in China: 2010-2050, Osteoporosis Int. 26 (7) (2015) 1929–1937, https://doi.org/10.1007/s00198-015-3093-2.
[4] G. Adami, A. Fassio, D. Gatti, O. Viapiana, C. Benini, M.I. Danila, et al., Osteoporosis in 10-year time: a glimpse into the future of osteoporosis, Ther Adv Musculoskel 20 (14) (2022) 1759720X–221083541X, https://doi.org/10.1177/1759720X221083541.
[5] A. Aibar-Almazan, A. Voltes-Martinez, Y. Castellote-Caballero, D.F. Afanador-Restrepo, M. Carcelen-Fraile, E. Lopez-Ruiz, Current status of the diagnosis and management of osteoporosis, Int. J. Mol. Sci. 23 (16) (2022), https://doi.org/10.3390/ijms23169465.
[6] Y. Tie-Lin, S. Anqi, D. Shan-Shan, Z. Deng, F. Zhao, A road map for understanding molecular and genetic determinants of osteoporosis, Nat. Rev. Endocrinol. 16 (2) (2020) 91–103, https://doi.org/10.1038/s41574-019-0282-7.
[7] V. Domazetovic, G. Marcucci, T. Iantomasi, M.L. Brandi, M.T. Vincenzini, Oxidative stress in bone remodeling: role of antioxidants, Clin Cases Miner Bone Metab 14 (2) (2017) 209–216, https://doi.org/10.11138/ccmbm/2017.14.1.209.
[8] M. Yishake, M. Yasen, L. Jiang, W. Liu, R. Xing, Q. Chen, et al., Effects of combined teriparatide and zoledronic acid on posterior lumbar vertebral fusion in an aged ovariectomized rat model of osteopenia, J. Orthop. Res. 36 (3) (2018) 937–944, https://doi.org/10.1002/jor.23682.
[9] Z. Bingkun, P. Qian, H.L.P. Enoch, C. Fubo, Z. Rong, S. Guangwei, et al., Leonurine promotes the osteoblast differentiation of rat BMSCs by activation of autophagy via the PI3K/Akt/mTOR pathway, Front Bioeng Biotechnol 9 (2021), 615191, https://doi.org/10.3389/fbioe.2021.615191.
[10] W. Le, L. Qiwang, B. Yuling, J. Xi, H. Menglin, Z. Kaiwen, et al., The relationship between oxidative stress and bone turnover in the elder people with osteoporosis, Chin J Osteoporosis 21 (2) (2015) 192–195, https://doi.org/10.3969/j.issn.1006-7108.2015.02.014.
[11] O. Altindag, O. Erel, N. Soran, H. Celik, S. Selek, Total oxidative/anti-oxidative status and relation to bone mineral density in osteoporosis, Rheumatol. Int. 28 (4) (2008) 317–321, https://doi.org/10.1007/s00296-007-0452-0.
[12] G. Banfi, E.L. Iorio, M.M. Corsi, Oxidative stress, free radicals and bone remodeling, Clin. Chem. Lab. Med. 46 (11) (2008) 1550–1555, https://doi.org/10.1515/CCLM.2008.302.
[13] J.A. Ardura, V. Alonso, P. Esbrit, P.A. Friedman, Oxidation inhibits PTH receptor signaling and trafficking, Biochem. Biophys. Res. Commun. 482 (4) (2017) 1019–1024, https://doi.org/10.1016/j.bbrc.2016.11.150.
[14] W. Shanshan, The Preparation of Collagen Peptides and Active Calcium from Cod Bone and its Preventive Effects on Osteoporosis, Ocean Univ China, 2013.
[15] L. Aubry, C. De-Oliveira-Ferreira, V. Santé-Lhoutellier, V. Ferraro, Redox potential and antioxidant capacity of bovine bone collagen peptides towards stable free radicals, and bovine meat lipids and proteins. Effect of animal age, bone anatomy and proteases-a step forward towards collagen-rich tissue valorisation, Molecules 25 (22) (2020) 5422, https://doi.org/10.3390/molecules25225422.
[16] Y. Kai, L. Ailing, H. Keguang, H. Zailin, C. Zhilin, C. Jing, et al., Sheep bone collagen peptide improve bone quality of ovariectomized rats, J Shanxi Agric (Nat Sci Ed) 39 (1) (2019) 102, https://doi.org/10.13842/j.cnki.issn1671-8151.201807019.
[17] Y. Mengliang, Z. Chunhui, J. Wei, S. Qingshan, Q. Xiaojie, Z. Hongru, et al., Metabolomics strategy reveals the osteogenic mechanism of yak (Bos grunniens) bone collagen peptides on ovariectomy-induced osteoporosis in rats, Food Funct. 11 (2) (2020) 1498–1512, https://doi.org/10.1039/c9fo01944h.
[18] W. Wenxia, Y. Tonghui, Z. Yi, W. Qingling, L. Shiling, L. Chengjiang, et al., Research progress on preparation and application in the food industry of bone collagen, Sci Technol Food Ind 43 (13) (2022) 445–454, https://doi.org/10.13386/j.issn1002-0306.2021070289.
[19] L. Jiayang, Z. Xiaofang, Research progress of livestock and poultry bone collagen and its peptides, Meat Ind 2021 (6) (2021) 51–57.
[20] M.C. Gómez-Guillén, B. Giménez, M.E. López-Caballero, M.P. Montero, Functional and bioactive properties of collagen and gelatin from alternative sources: a review, Food Hydrocoll 25 (8) (2011) 1813–1827, https://doi.org/10.1016/j.foodhyd.2011.02.007.
[21] Y. Xiurong, Z. Yuqin, Q. Yiting, C. Changfeng, Wang. Bin, Preparation and characterization of gelatin and antioxidant peptides from gelatin hydrolysate of skipjack tuna (Katsuwonus pelamis) bone stimulated by in vitro gastrointestinal digestion, Mar. Drugs 17 (2) (2019) 78, https://doi.org/10.3390/md17020078.

[22] L. Feng, W. Wencheng, X. Yunqiu, C. Xuehong, H. Yantao, M. Desen, et al., Protection by collagen peptides from walleye pollock skin on bone formation via inhibition of oxidative stress, J. King Saud Univ. Sci. 32 (5) (2020) 2527–2533, https://doi.org/10.1016/j.jksus.2020.03.006.
[23] F. Yumei, S. Chuanchao, T. Hang, Z. Xiaohan, Z. Haiqing, L. Feng, Study on the nutritional ingredients and the effect on the repair of damaged skin barrier function of donkey bone collagen, Sci Technol Food Ind 42 (23) (2021) 341–349, https://doi.org/10.13386/j.issn1002-0306.2021010211.
[24] Z. Guangyun, F. Yumei, L. Chuyi, L. Feng, Z. Xiaohan, L. Bafang, Effect of donkey bone collagen peptide on improving osteoporosis in rats, Sci Technol Food Ind 42 (22) (2021) 336–343, https://doi.org/10.13386/j.issn1002-0306.2020120031.
[25] Q. Zhifei, L. Weiwei, Z. Yingchun, Y. Yuwen, Antioxidant and antibacterial activity of donkey bone seasoning and its application in ready-to-eat patties, Meat Res 34 (11) (2020) 32–37, https://doi.org/10.7506/rlyj1001-8123-20201005-237.
[26] Q. Shanshan, Research progress of osteoporosis disease animal model, Heilongjiang Anim. Sci. Vet. Med. (9) (2016) 96–98, https://doi.org/10.13881/j.cnki.hljxmsy.2016.0776.
[27] W. Yi, H. Yusheng, X. Lina, M. Shuang, L. Qin, Construction of D-galactose combined with low calcium diet induced bone mass reduction model in mice, J Tradi Chin Vet Med 41 (2) (2022) 15–19, https://doi.org/10.13823/j.cnki.jtcvm.2022.02.003.
[28] R. Geyi, M. Xuelian, P. Li, Q. Haiwen, B. Malacuo, Z. Shuyao, et al., Structural characteristics of bovine bone collagen under different extraction processes, Sci Technol Food Ind 43 (14) (2022) 27–33, https://doi.org/10.13386/j.issn1002-0306.2021090282.
[29] O. Blokhina, E. Virolainen, K.V. Fagerstedt, Antioxidants, oxidative damage and oxygen deprivation stress: a review, Ann Bot-London 91 (2) (2003) 179–194, https://doi.org/10.1093/aob/mcf118.
[30] L. Qinghui, H. Zhen, C. Dehong, Differentiation of rat bone marrow mesenchymal stem cells into osteoblasts following induction of ascorbic acid, beta-sodium glycerophosphate and dexamethasone, J Clin Rehabil Tissue Eng Res 13 (1) (2009) 88–91.
[31] W. Zhanjing, W. Wenqi, Z. Yuanyuan, L. Jianfeng, Exploration on the preparation of CT samples of isolated mouse femoral trabecular bone and cortical bone, J Med Inf 35 (12) (2022) 118–121, https://doi.org/10.3969/j.issn.1006-1959.2022.12.028.
[32] W. Zhanying, Z. Zhenlin, Interpretation and application of Micro-CT to obtain microstructure index in bone metabolism research, Chin J Osteoporosis Bone Miner Res 11 (2) (2018) 200–205, https://doi.org/10.3969/j.issn.1674-2591.2018.02.016.
[33] Z. Yazhen, Z. Hongguang, Establishment and measurement of D-galactose induced aging model, Fudan Univ. J. Med. Sci. 34 (4) (2007) 617–619.
[34] T. Qiaoyan, Z. Haichao, L. Shenglai, Y. Jiarong, K. Shaosong, Comparison of the primary organ coefficients of the SPF grade with the ordinary grade Hartley Guinea pig, Lab. Anim. Sci. 30 (6) (2013) 31–33.
[35] Z. Tiannong, L. Dandan, T. Lihai, W. Yan, L. Liangfeng, L. Ping, et al., Experimental study on Hepatic-protective effects of radix millettiae speciosae, Lishizhen Med Mater Med Res 20 (10) (2009) 2585–2587.
[36] W. Jingyuan, Z. Xinmu, Z. Ronghai, Z. Yulai, Y. Weiqun, Protective effect of aprotinin on acute liver injury induced by D-GalN, J. Mol. Sci. 23 (3) (2007) 194–197, https://doi.org/10.13563/j.cnki.jmolsci.2007.03.010.
[37] T. Kuo, C. Chen, Bone biomarker for the clinical assessment of osteoporosis: recent developments and future perspectives, Biomark. Res. 5 (2017) 18, https://doi.org/10.1186/s40364-017-0097-4.
[38] L. Chuntong, K. Xinxin, G. Jianhui, W. Qiming, L. Shutao, G. Jingke, et al., A preliminary study on the antioxidant relationship between collagen and collagen peptides, J. Chin. Inst. Food Sci. Technol. 17 (10) (2017) 44–50, https://doi.org/10.16429/j.1009-7848.2017.10.007.
[39] C. Changfeng, C. Zihao, W. Bin, H. Fayuan, L. Zhongrui, Z. Bin, Antioxidant and functional properties of collagen hydrolysates from Spanish mackerel skin as influenced by average molecular weight, Molecules 19 (8) (2014) 11211–11230, https://doi.org/10.3390/molecules190811211.
[40] S. Himaya, B.M. Ryu, D.H. Ngo, S.K. Kim, Peptide isolated from Japanese flounder skin gelatin protects against cellular oxidative damage, J. Agric. Food Chem. 60 (36) (2012) 9112–9119, https://doi.org/10.3390/molecules190811211.
[41] R. Jiaoyan, Z. Mouming, C. Chun, Y. Lijun, W. Hhaiyan, Isolation and identification of antioxidant peptides from hydrolyzed grass carp protein, Food Sci. (N. Y.) 30 (13) (2009) 13–17.
[42] W. Yiping, C. Tao, R. Jianwei, P. Weiwei, The protective effect of 3,4-dihydroxy acetophenone on H_2O_2-induced osteoblastic MC3T3-E1 cells injury, Jiangsu Med. J. 46 (8) (2020) 765–769, https://doi.org/10.19460/j.cnki.0253-3685.2020.08.003.